Supplementary Information

Supplementary Figures

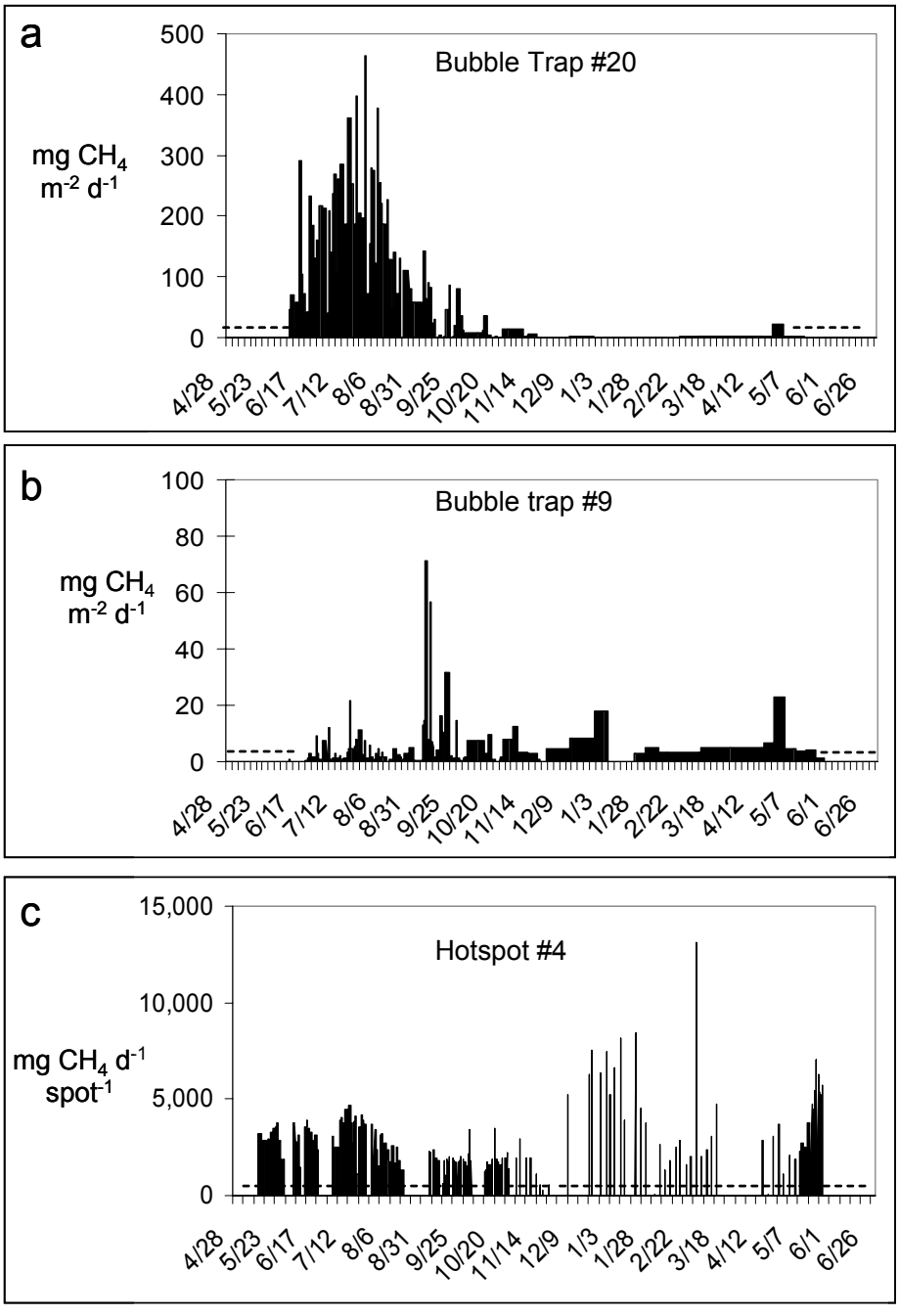

Supplementary Figure 1. Ebullition dynamics captured by daily measurements during 2003-04 in single bubble traps floating at randomly located points where water was 2-m deep (a) and 10-m deep (b). We secured traps over individual hotspots (c). In summer, hotspot traps were sampled daily as they filled often with >15L of gas each day; but in winter when logistics necessitated less frequent sampling, we measured hotspot fluxes over the course of several hours to prevent umbrellas from overflowing and freezing into the ice. We verified that hourly flux rates were not different from daily flux rates. Dashed lines represent periods of 'no-data'.

Supplementary Figure 2. Photograph of hotspots along thermokarst lake margin. Methane emissions along thermokarst margins (128 g CH4 m-2 yr-1) exceeded whole lake average emissions (24.9 g CH4 m-2 yr-1) in the

intensively studied lakes because of a higher abundance of hotspots and point sources of ebullition in the thermokarst zone. Hotspots in the photograph, which was taken in October 2003 at Shuchi Lake, are open holes in ice inside the dark rings of wet snow.

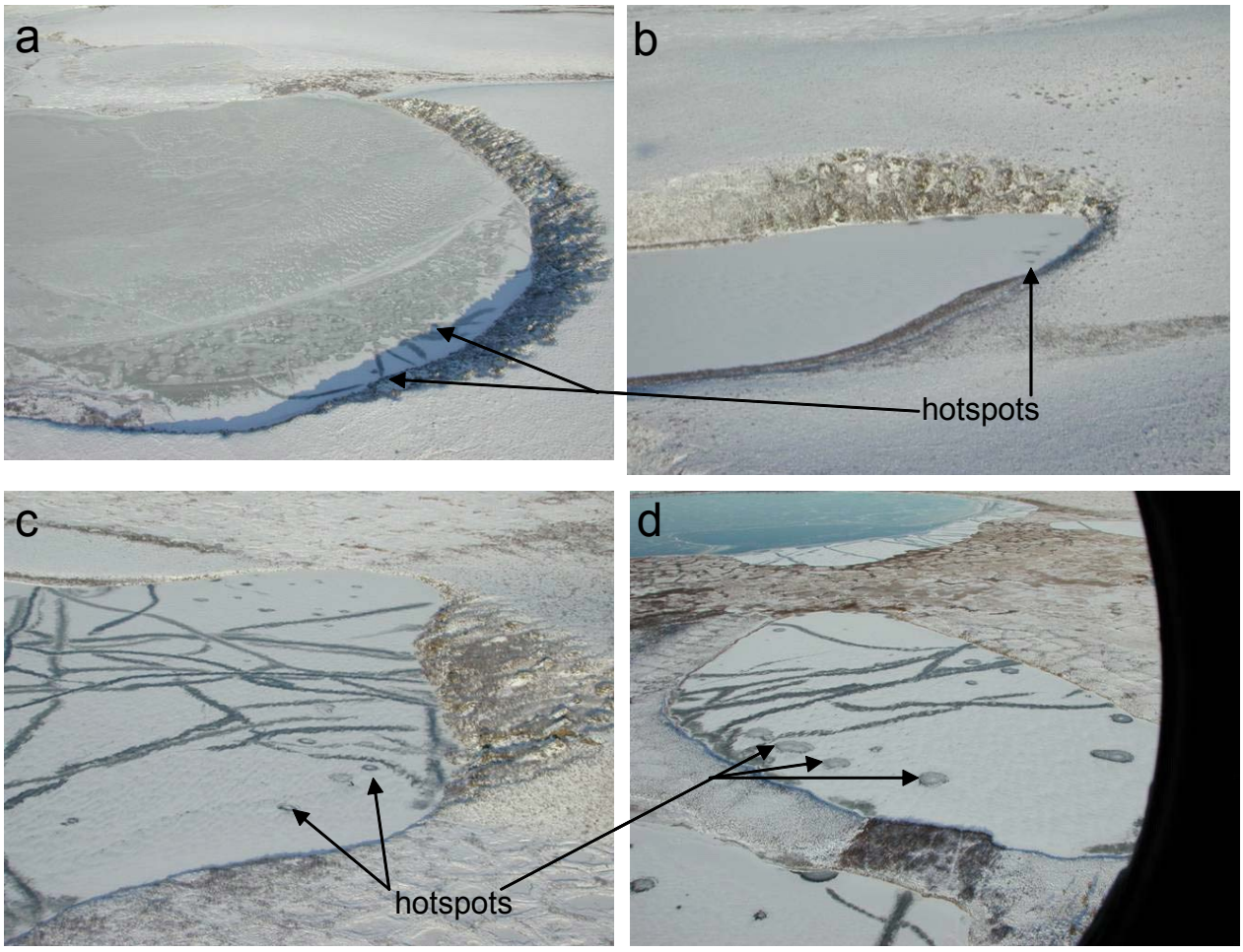

Supplementary Figure 3. Black-hole hotspots (dark round spots) mark the zone of enhanced methane emissions due to thermokarst erosion. We sorted aerial photographs of 60 lakes into two categories reflecting lakes with moderate and intense thermokarst erosion. Half of the lakes exhibited moderate erosion, with black-hole hotspots occurring primarily in a narrow zone 15-m from the thermokarst margin (panels *a* and *b*, as well as our two intensively studied lakes). This zone was 15.8 ± 2.2% of lake area in our intensively studied lakes.

Black-hole hotspots extended >30-m into the lake away from thaw margins in the other half of the photos (panels c and d), suggesting that these lakes have a recent history of more intense thermokarst erosion. Due to a lack of coordinates for lakes in aerial photographs we were unable to directly link the GIS lake change analysis to hotspot distributions in the photographs. To extrapolate CH4 fluxes to these lakes, we applied flux rates measured along thermokarst margins of our intensive study lakes (128 g CH4 m-2 yr-1) to a doubly large zone of thermokarst influence (31.6% of lake area).

Supplementary Figure 4. Large, rare emission events. Some CH_4 emission events are unpredictable, but may be of large magnitude. Three times we observed geysers of lake gas released during a >30-second episode, which created an eruption cone that stood several centimeters above the lake water surface (not shown). In August of 2002 and 2003 we used video and photography to document large plumes of CH_4 that lifted thick peat mats (12 m^2) from the bottom of thermokarst lakes 4-8 m to the surface (below). These lake bottom islands floated at the lake surface for 3-6 days releasing CH_4, before sinking back to the lake bottom. Methane bubbled out from the mat when we disturbed it with a pole.

Supplementary Methods

Methane concentration and isotope analysis of ebullition measured by bubble traps

During winter, we measured every 3-4 days the volume of gas collected continuously in bubble traps suspended beneath the ice. Measurements were daily during the ice-free season. In total, we made 2,981 individual measurements of bubble volumes collected in bubble traps. Methane concentration of bubbles was 79.6 ± 1.1% CH_4 (n=36), as measured by gas chromatography using a thermal conductivity detector (TCD Shimadzu 8A) and a flame ionization detector (FID Shimadzu 6A). For isotope analyses, gas samples were collected directly into glass serum vials from ebullition flux, sealed with Butyl rubber stoppers, and stored at 4° C. We measured $^{13}C/^{12}C$ of CH_4 by direct injection with a syringe using gas chromatography/mass spectrometry (Hewlet-Packard 5890 Series II GC coupled to a Finnigan MAT Delta S). A subsample of gas was combusted to CO_2 and catalytically reduced to graphite[31], and its $^{14}C/^{12}C$ values

measured by atomic mass spectrometry at the Keck Carbon Cycle AMS Facility at the University of California, Irvine. We determined D/H of CH_4 on a Finnigan MT delta +XP using a Trace GC with a poroplot column and the reduction column set at 1450°C.

Methane fluxes from point sources and hotspots

We made detailed, continuous measurements of three categories of point sources identified by distinct patterns of bubble stacks in lake ice from 10/9-10/29/2003 (n=6-8 traps per category): *kotenok* (stacks of small individual, unmerged bubbles, 25 ± 12 mg CH_4 d^{-1} $spot^{-1}$), *koshka* (merged bubbles clustered in multiple layers of ice, 190 ± 172 mg CH_4 d^{-1} $spot^{-1}$), *kotara* (single large pockets of merged bubbles in ice, 825 ± 348 mg CH_4 d^{-1} $spot^{-1}$) and open-hole *hotspots* (2175 ± 1195 mg CH_4 d^{-1} $spot^{-1}$) (ANOVA, $F=16.23_{3,27}$ $p<.0001$) (Fig. 1). Unlike other point sources, seasonal averages for hotspots were derived from year-round measurements using bubble traps (1754 ± 690 mg CH_4 d^{-1} $spot^{-1}$, n=4 traps summer; 2125 ± 1222 mg CH_4 d^{-1} $spot^{-1}$, n=10 traps winter). In contrast, average flux by molecular diffusion was 10 ± 1.8 mg CH_4 m^{-2} d^{-1} during the summer.

The CH_4 concentration in point-source bubbles trapped in lake ice in spring before any thawing occurred (53.6 ± 1.6 % CH_4; n=3) was similar to earlier observations (50% CH_4, n=8 koshkas)[3] and 33% less than in fresh lake bubbles (80%). When applying CH_4 concentrations to the bubble volume measurements, we used 54% CH_4 in our calculation of wintertime 'point-source' and 'background' ebullition, and 80% for all other ebullition.

Supplementary Equations

Whole lake emission estimation

We estimate whole-lake CH_4 emissions M_{1tot} as the average of two intensively studied lakes, (24.9 ± 2.3 mg CH_4 m^{-2} yr^{-1}): where

$$M_{1tot} = \sum_{z=1}^{3} A_z \left(M_{dz} + M_{hz} + M_{pz} + M_{bz} \right) \quad (1)$$

z = The 3 major lake zones: shallow thermokarst margins, non-thermokarst margins, and the deeper center of lakes.

A_z = area of each zone (fraction of lake area).

M_d = Diffusive flux estimated from biweekly surface water concentrations of CH_4 measured during the ice-free summer period in the lake center[14] (mg CH_4 m^{-2} yr^{-1}).

M_h = Density of hotspots (No. points m^{-2}) * mean flux per hotspot (mg CH_4 $season^{-1}$) for summer (n=4 hotspots) and winter (n=10 hotspots).

$$M_p = t \sum_{s=1}^{3} \rho_s M_s \quad (2)$$

where ρ_s is the density of each point source (No. points m^{-2}, s = point source type: kotenok (1), koshka (2), or kotara (3); M_s is the mean flux per point source (mg CH_4 day^{-1} in October; n = 6-8 traps per point source type); and t is 365 days per year. This extrapolation is conservative because October point source ebullition appeared to be lower than at other times of year (data not shown).

M_b = Average seasonal bubble fluxes determined for randomly situated traps (background ebullition) as a summation of interpolation of daily fluxes during winter and summer. Background traps were monitored year round with 2-10 traps per lake zone. The complete table of North Siberian methane emission sources detailed for each lake is provided in Supplementary Information.

Regional extrapolation

Regional estimates M_{yedoma} (3.8 Tg CH_4 yr^{-1}) were extrapolated from whole lake fluxes as follows:

$$M_{yedoma} = A_{yedoma} * P_{lakes} * 0.5(M_{1tot} + M_{2tot}) \quad (3)$$

Where A_{yedoma} is $1x10^6$ km^2; P_{lakes} is 0.11 fractional lake cover; M_{1tot} is 24.9 g CH_4 m^{-2} yr^{-1}, representing half of the region's lakes with modest erosion; and M_{2tot} is 43.7 CH_4 m^{-2} yr^{-1}, the flux from the other half of the region's lakes with intense thermokarst erosion and extensive hotspots.

This 11% lake cover estimate, based on our GIS analysis, is conservative relative to the range reported in the literature (8.5 to >30%) (ref. 3,9,23). To lend support to the assumption that our estimates of CH_4 flux are representative, we verified that 2003-2004 had temperature and precipitation inputs typical of the study period, 1970-2004, based on observations made at the Cherskii Meteorological Station (data not shown). The mean annual temperature during 2003-2004 spans the current trend line for this region[28] (Fig. 3).

Supplementary Tables

Supplementary Table 1. Sources of variability in our estimate of Siberian thaw lake CH_4 emissions for yedoma territory. By documenting ebullition patchiness, we were able to assess sources of uncertainty in our regional estimate of CH_4. Within-lake sources of variability, such as errors associated with point source fluxes, led to a smaller range of variability for regional estimates (2.4-5.1 Tg CH_4 yr^{-1}) than percentage of the region occupied by lakes (2.9-10.3 Tg CH_4 yr^{-1}). Since our extrapolation is based on the conservative estimate of lake area, actual regional emissions could be higher.

Calculations are based on mean values of point source density per unit lake area and the mean flux per point source type in our intensively studied lakes. Here we present the potential effect of the largest sources of variability around the whole-lake and regional means (34.3 g CH_4 m^{-2} yr^{-1}, 3.8 Tg CH_4 yr^{-1}) that are not accounted for in Equations 1-3, assuming that emissions from half of the region's lakes are the same as our study lakes (24.9 g CH_4 m^{-2} yr^{-1} with 15.8% thermokarst zone area), and emissions from the other half of the region's lakes reflect a 2-times larger thermokarst zone (43.7 g CH_4 m^{-2} yr^{-1} with 31.6% thermokarst zone area). Since lake area (as a percent of the yedoma region) is the largest source of variability influencing regional estimates of lake CH_4 emissions, we used a low-end estimate (11% lake area) in our calculations to be conservative. Other potential sources of variation that we have not estimated include the areal extent of yedoma, CH_4 flux and thermokarst erosion variation among lakes in different yedoma sub-regions, intra-lake flux variation for lakes with intense erosion, and interannual variation.

Source of variability	Range of variability	Intensive study lakes g CH_4 m^{-2} yr^{-1}	Average regional lakes g CH_4 m^{-2} yr^{-1}	Regional flux Tg CH_4 yr^{-1}
Flux per point source[†]	36%	16.0 to 33.5	21.6 to 46.5	2.4 to 5.1
Density of point sources[α]	16%	22.9 to 31.4	30.4 to 42.2	3.3 to 4.6
Between zones within lakes[β]		*Accounted for in calculations*		
Between intensive study lakes	9%	22.7 to 27.2		
Between lakes with modest *vs*. intense thermokarst		*Accounted for in calculations*		
Lake area (percent of region)[γ]	46%			2.9 to 10.3

† The range shown in the table is the mean flux minus the standard deviation for each point source category in each lake zone and the mean flux plus the standard deviation for each point source category in each lake zone using the mean density of point source types—i.e., the variation in flux among replicate bubble traps for a given point source type in a given lake zone.

α The range shown in the table applies the mean flux for each point source category to the mean density minus the standard deviation of density for each point source type in each lake zone and the mean density plus the standard deviation of density for each point source type in each lake zone—i.e., the variation in flux due to variation in density of a given point source type in a given lake zone.

β We accounted for variation between zones in our calculations (Supplementary Table 2). Methane emissions from the zone of shallow thermokarst margins had the highest flux.

γ Lake area estimates for sub-regions of yedoma territory are reported as 8.5% to >30%.

Supplementary Table 2. Detailed calculation of annual CH_4 emissions from two intensively studied lakes. Whole-lake methane emissions are the area-weighted sum of emissions for each zone of the lake (thermokarst margins, deep center, and non-thermokarst margins). Methane fluxes are the sum of molecular diffusion and ebullition. The patchiness of ebullition is accounted for by quantifying 'background', 'point-source' and 'hotspot' bubbling. We calculated emission estimates for half of the region's lakes with intense thermokarst erosion, which are not represented by our intensive study lakes, by doubling the area of thermokarst zones in this table and subtracting the difference from the deep center zone.

Lake	Zone within lake	Area	% Annual emissions	Area weighted ← mg CH_4 m^{-2} yr^{-1} summer	Area weighted ← mg CH_4 m^{-2} yr^{-1} winter	Subsection = mg CH_4 m^{-2} yr^{-1} summer	Subsection = mg CH_4 m^{-2} yr^{-1} winter	Diffusion + mg CH_4 m^{-2} yr^{-1} summer	Hotspots + mg CH_4 m^{-2} yr^{-1} summer	Hotspots + mg CH_4 m^{-2} yr^{-1} winter	Point sources + mg CH_4 m^{-2} yr^{-1} summer	Point sources + mg CH_4 m^{-2} yr^{-1} winter	Background mg CH_4 m^{-2} yr^{-1} summer	Background mg CH_4 m^{-2} yr^{-1} winter	Bubble traps n
Tube	Thermokarst	14%	76%	11,733	8,910	86,272	65,515	1,213	9,316	18,782	34,066	46,026	41,677	707	3
Dispenser	Deep center	81%	21%	3,891	1,768	4,828	2,193	1,213	182	366	1,049	1,417	2,384	410	6
	Non-thermokarst	6%	3%	409	507	7,046	8,739	1,213	3,838	7,739	184	248	1,811	752	2
	Whole lake	100%	100%	16,033	11,185			1,213	1,636	3,298	5,489	7,416	7,695	471	
	% of annual flux			59%	41%			4%	18%		47%		30%		
	Total			27,218				1,213	4,934		12,905		8,165		
Shuchi	Thermokarst	18%	82%	9,337	9,355	51,889	51,986	1,425	1,448	3,450	35,369	47,786	13,647	750	2
	Deep center	79%	17%	2,694	1,065	3,410	1,349	1,425	42	101	601	812	1,342	436	10
	Non-thermokarst	3%	1%	162	45	5,373	1,480	1,425	111	264	309	417	3,528	799	2
	Whole lake	100%	100%	12,193	10,465			1,425	297	709	6,849	9,253	3,622	503	
	% of annual flux			54%	46%			6%	4%		71%		18%		
	Total			22,658				1,425	1,006		16,101		4,126		

Supplementary Notes

Reference

31. M. Stuiver, M. & H. Polach. Reporting of ^{14}C data. *Radiocarbon.* **19**, 355-363 (1977).